






Two-mode terms in Wigner transport equation elucidate anomalous thermal transport in amorphous silicon

Jin Yang ¹, Xueyan Zhu ^{2,3}, Alan J. H. McGaughey ⁴, Yee Sin Ang ⁵, and Wee-Liat Ong ^{1,6,*}

¹ZJU-UIUC Institute, College of Energy Engineering, Zhejiang University, Jiaxing, Haining, Zhejiang 314400, China

²China Academy of Engineering Physics Software Center for High Performance Numerical Simulation, Beijing 100088, China

³Institute of Applied Physics and Computational Mathematics, Beijing 100088, China

⁴Department of Mechanical Engineering, Carnegie Mellon University, Pittsburgh, Pennsylvania 15213, USA

⁵Science, Mathematics and Technology, Singapore University of Technology and Design, 487372 Singapore

⁶State Key Laboratory of Clean Energy Utilization, Zhejiang University, Hangzhou, Zhejiang 310027, China



(Received 18 October 2024; revised 27 January 2025; accepted 10 March 2025; published 20 March 2025)

Over the past decades, our understanding of thermal transport in amorphous materials has predominantly relied on the inherently harmonic Allen-Feldman theory, which has been found to be insufficient. In this study, the Wigner transport formalism is adopted to explicitly account for anharmonicity. In studying the thermal transport in amorphous silicon, the results highlight that amorphous materials are not generally computationally equivalent to crystals with disordered primitive cells. A method that leverages the properties of the two-mode terms in the Wigner transport formalism is proposed to predict the bulk thermal conductivity of amorphous materials using finite-size models. In doing so, the need for mode classification schemes required in the Allen-Feldman theory is eliminated, and similarities are discovered between the two-mode terms and the carriers commonly used to describe thermal transport in amorphous materials, i.e., propagons, diffusons, and locons. Two competing trends are identified that shed light on the recently discovered anomalous decrease in the high-temperature thermal conductivity in some amorphous materials.

DOI: [10.1103/PhysRevB.111.094206](https://doi.org/10.1103/PhysRevB.111.094206)

I. INTRODUCTION

Amorphous materials play a vital role in diverse technological sectors, powering nanoscale electronics [1], enabling affordable solar energy [2], reclaiming waste heat [3], and serving as a cornerstone in optics industries [4]. The thermal transport characteristics of these materials are paramount in influencing the efficiency and durability of the associated devices. However, our comprehension of the heat carriers in this class of materials frequently hinges on the decades-old yet incomplete Allen-Feldman (AF) theory [5], leaving ample space for improvements.

As a heat carrying vibrational mode in an amorphous material may have a mean free path (ℓ) smaller than its wavelength (λ) or the interatomic spacing (a), the applicability of the term “phonon” becomes questionable [6–9]. Consequently, the terminology of “propagons” (i.e., low-frequency propagating modes that adhere to the phonon-gas model), “diffusons” (i.e., nonpropagating but delocalized modes), and “locons” (i.e., localized modes with zero diffusivity under the harmonic approximation) became accepted [8,9]. Thus, calculating the total thermal conductivity of an amorphous material required *a priori* categorization of the vibrational modes and methods for obtaining their contributions to thermal conductivity. The AF theory, for example, calculates the thermal conductivity contribution from diffusons using a formula derived from Kubo theory under the harmonic approximation [5].

Despite significant progress in past decades, ambiguities in classifying the three heat carriers persist, which impacts their relative contributions to thermal conductivity [8–22]. Often, a frequency crossover (ω_c) is used to distinguish propagons and diffusons. Because ω_c lacks a precise definition, thermal transport studies on amorphous materials usually employ *ad hoc* criteria for determining ω_c , leading to inconsistencies between their results [7–10]. Considering the example of amorphous silicon (a-Si), different approaches have been used to define ω_c , the angular frequency-dependent linewidth of propagons [$\Gamma_p(\omega)$] to account for anharmonic scattering, and the propagon velocity (v_p). Different choices have led to a substantial disparity in the relative contribution of propagons to the total thermal conductivity of a-Si, ranging from 25% to 90% at room temperature [7–9,12,13,17,21]. A similar controversy exists in using the mobility edge to distinguish diffusons from locons due to different methods used for determining the edge location [7–9,14,16,23–26]. Although Green-Kubo modal analysis-based results for a-Si concur with previous studies to show negligible thermal conductivity contributions from participation ratio (PR)-determined locons [15], such PR-determined locons can contribute appreciably in amorphous silica (a-SiO₂) and polymers [23,25,26].

Recently, different groups revisited the heat flux operator [27] and proposed unified thermal transport theories for crystalline and amorphous solids, namely, the Wigner transport equation [28] (WTE) and the quasiharmonic Green-Kubo (QHKG) theory [29]. The WTE encompasses the wave nature of phonon transport, allowing phonons with a mean free path below the spatial Ioffe-Regel limit (i.e., a mean free

*Contact author: weeong@intl.zju.edu.cn

path less than the interatomic spacing, $\ell < a$) to transfer heat through a “coherence channel” and still be considered as well-defined entities [28,30]. Simoncelli and co-workers [31–33] later applied the WTE with the Voigt regularization protocol to several amorphous materials and alloys. This regularization protocol avoids the divergence of the low-temperature thermal conductivities predicted by the WTE with a finite Brillouin zone \mathbf{k} -point sampling. Their work concluded that glasses can be computationally regarded as crystals with disordered primitive cells, making classification of the heat carriers and models for calculating their contribution to thermal conductivity unnecessary, as also implied in an earlier study [34]. On the other hand, others continue to assert that amorphous materials are computationally not similar to crystals. In their study of a-Si, a-SiO₂, and amorphous silicon carbide, Fiorentino *et al.* used the QHGK approach to include anharmonicity in determining the thermal conductivity contributions from diffusons and locons, but argued that the contributions of propagons should be addressed separately [21,35]. Despite this recent progress, further analysis can clarify the use of these methods on different amorphous materials for accelerating the convergence of thermal conductivity calculations.

To address the above issues, we conducted numerical calculations on a-Si with the Stillinger-Weber (SW) potential [36]. This potential has been successfully employed in prior studies for a-Si [5,7–10,13,15,17]. The structure of this paper is as follows: we first determine that a-Si cannot be treated as a crystal with a disordered primitive cell for thermal conductivity calculations. Then, we demonstrate that by leveraging the properties of the two-mode terms in the WTE, it is sufficient to obtain the bulk thermal conductivity of a-Si using a finite-size model, without invoking any other assumptions. Next, we discuss a possible relationship of the two-mode terms in the WTE with propagons, diffusons, and locons. Finally, we illustrate how our framework naturally captures and explains the a-Si thermal conductivity trend across temperatures, and notably the recently discovered anomalous decrease at high temperatures.

II. METHODS

A. Unified theories for amorphous materials

The unified theories (i.e., WTE and QHGK) can describe thermal transport in crystals and amorphous materials. Although their final expressions differ due to the nonuniqueness of the heat flux operator and approximation schemes used, subsequent studies have confirmed negligible differences in their results in the quasiparticle regime ($\Gamma < \omega$) [30,37,38]. Focusing on the WTE, its thermal conductivity expression is written as [30,37]

$$\begin{aligned} \kappa &= \frac{1}{3V} \sum_{\mathbf{k}} \sum_{s,s'} \kappa(\mathbf{k})_{s,s'} \\ &= \frac{1}{3V} \sum_{\mathbf{k}} \sum_{s,s'} \frac{\omega(\mathbf{k})_s + \omega(\mathbf{k})_{s'}}{4} \left(\frac{C(\mathbf{k})_s}{\omega(\mathbf{k})_s} + \frac{C(\mathbf{k})_{s'}}{\omega(\mathbf{k})_{s'}} \right) \\ &\quad \times \|\mathbf{v}(\mathbf{k})_{s,s'}\|^2 \frac{[\Gamma(\mathbf{k})_s + \Gamma(\mathbf{k})_{s'}]/2}{[\omega(\mathbf{k})_s - \omega(\mathbf{k})_{s'}]^2 + [\Gamma(\mathbf{k})_s + \Gamma(\mathbf{k})_{s'}]^2/4}, \end{aligned} \quad (1)$$

where the wave vector \mathbf{k} and the indexes s and s' distinguish vibrational modes, V is the volume, and $\omega(\mathbf{k})_s$, $\Gamma(\mathbf{k})_s$, and $C(\mathbf{k})_s$ are the angular frequency, linewidth, and heat capacity of a vibrational mode $(\mathbf{k})_s$. $C(\mathbf{k})_s = \frac{\hbar^2 \omega^2(\mathbf{k})_s}{k_B T^2} \frac{\exp[\hbar \omega(\mathbf{k})_s / k_B T]}{(\exp[\hbar \omega(\mathbf{k})_s / k_B T] - 1)^2}$ for quantum statistics and $C(\mathbf{k})_s = k_B$ for classical statistics. The quantity $\|\mathbf{v}(\mathbf{k})_{s,s'}\|^2 = \sum_{\alpha=x,y,z} |v^\alpha(\mathbf{k})_{s,s'}|^2$ where $v^\alpha(\mathbf{k})_{s,s'}$ is the two-mode group velocity of vibrational modes $(\mathbf{k})_s$ and $(\mathbf{k})_{s'}$ along the Cartesian α direction [33]. The WTE captures the particle-wave duality inherent in the transport process using the interband ($s \neq s'$) coherence-channel transport for the wavelike tunneling and the intraband ($s = s'$) population-channel transport for the particlelike propagation [28,30].

Theoretically, an infinitely large primitive cell is needed for studying an amorphous material. Computational constraints, however, restrict the possible size, leading to missing contributions from low-frequency modes [6]. Two approaches have been proposed to address this issue [6,33]: (1) treating nonperiodic glasses as crystals with disordered primitive cells and evaluating the thermal conductivity using a small, finite Brillouin zone (herein, the \mathbf{k} -mesh approach); and (2) only considering vibrational modes at the Gamma point (i.e., the center of the Brillouin zone where $\mathbf{k} = \mathbf{0}$) and adding the missing contributions from propagons, with their properties extrapolated from the density of states (DOS) $[N(\omega)]$ and linewidth $[\Gamma_p(\omega)]$ [7–9]. Consequently, the total thermal conductivity (κ_T) is the sum of contributions from propagons κ_P and diffusons/locons $\kappa_{D/L}$, giving

$$\begin{aligned} \kappa_T &= \kappa_P + \kappa_{D/L} \\ &= \frac{v_s^2}{3V} \int_0^{\omega_c} N(\omega) C(\omega) \frac{1}{\Gamma_p(\omega)} d\omega \\ &\quad + \frac{1}{V} \sum_{s,s'} \Theta(\omega_{s/s'} - \omega_c) \kappa_{s,s'}, \end{aligned} \quad (2)$$

where ω_c is the crossover frequency to classify propagons and diffusons, and v_s is the sound speed. $\Theta(\omega_{s/s'} - \omega_c) = 1$ if ω_s or $\omega_{s'}$ is larger than ω_c and $\Theta(\omega_{s/s'} - \omega_c) = 0$ otherwise. We emphasize that anharmonicity is effectively accounted for when $\kappa_{s,s'}$ is calculated using the WTE [Eq. (1)] instead of the AF theory. A more straightforward approach than Eq. (2) to get the bulk thermal conductivity is to enlarge the primitive cell successively and calculate the corresponding thermal conductivity using only the Gamma-point modes with Eq. (1), and then extrapolate to an infinite system size (herein, the Gamma-point approach).

B. Generating a-Si models

In the Gamma-point approach, a melt-quench technique [17] was used to generate models with different numbers of atoms (from 216 to 46 656). In the \mathbf{k} -mesh approach, the 216-atom primitive cell was replicated $N \times N \times N$ in space to generate supercell models with the same number of atoms as the Gamma-point models. It should be noted that the WTE thermal conductivity obtained using a supercell model in the Gamma-point approach yields the same result as that obtained using the primitive cell with a \mathbf{k} -mesh approach [39]. To reduce computational cost in the \mathbf{k} -mesh approach, the primitive cell was employed with its \mathbf{k} -mesh size set as $N \times N \times N$ to

match the size of the supercell model [39]. For example, if the Gamma-point approach uses a supercell model which is a $3 \times 3 \times 3$ expansion of the primitive cell, the \mathbf{k} -mesh approach uses the primitive cell with the \mathbf{k} -mesh size set as $3 \times 3 \times 3$.

The molecular dynamics (MD) calculations were executed using LAMMPS [40,41] with a time step of 0.5 fs and periodic boundary conditions were applied in all directions. Initial structures were formed by melting crystalline silicon at 3500 K for 1 ns in the *NVT* ensemble utilizing a Nose-Hoover thermostat. Subsequently, the liquid silicon underwent quenching to 1000 K with a quench rate of 100 K ps⁻¹, followed by annealing at 1000 K for 25 ns to mitigate metastabilities. Lastly, the domain was quenched at a rate of 100 K ps⁻¹ to 300 K and stabilized at 300 K for 10 ns in the *NVT* ensemble. The resulting average density of the samples is 2351 ± 7 kg m⁻³, which agrees well with previous calculations and experiments [13,42]. The radial distribution functions are calculated using LAMMPS in the *NVE* ensemble at 300 K.

C. Molecular dynamics simulations for thermal conductivity

Equilibrium molecular dynamics (EMD) simulations were carried out in LAMMPS with a time step of 0.5 fs. The structures were initially equilibrated at 300 K for 0.5 ns in the *NVT* ensemble and then in the *NVE* ensemble for another 0.5 ns. Subsequently, the heat flux was computed for 10 ns in the *NVE* ensemble to determine the thermal conductivity. Homogeneous nonequilibrium molecular dynamics (HNEMD) simulations and their spectral decomposition were performed using GPUMD [43,44]. The above equilibration protocol was also applied for the HNEMD calculations, with a driving force parameter of 10^{-4} Å⁻¹. In the spectral heat flux calculations, the data was collected every two time steps, and the maximum correlation time used was 500 fs. Five independent runs were averaged for each EMD point and three for each HNEMD point.

D. Harmonic lattice dynamics calculations and normal mode decomposition method

The structures were initially optimized using the conjugate gradient algorithm in LAMMPS. Subsequently, the finite difference method implemented in PHONOPY [45,46] was employed to calculate the harmonic interatomic force constants. The vibrational frequencies, eigenvectors, and DOS were also computed from PHONOPY. For the normal mode decomposition (NMD) calculations that require time-dependent atomic velocities, *NVE* simulations were performed for 1 ns using a time step of 0.5 fs in LAMMPS after the structure relaxation. The atomic velocities were dumped with an interval of 12.5 fs. The spectral energy density for a specific vibrational mode (\mathbf{k})_s is given as [47–49]

$$\Phi(\mathbf{k}, \omega)_s = \left| \int_0^{+\infty} \dot{q}(\mathbf{k}, t)_s \exp(-i\omega t) dt \right|^2, \quad (3)$$

$$\dot{q}(\mathbf{k}, t)_s = \sum_{\alpha}^3 \sum_b^n \sum_l^{N_p} \sqrt{\frac{m_b}{N_p}} v_{l,b,\alpha}(t) e_{b,\alpha}^*(\mathbf{k})_s \exp(i\mathbf{k} \cdot \mathbf{r}_{l,b}^0), \quad (4)$$

where n is the number of atoms in one primitive cell, N_p is the number of primitive cells in the model, v is the velocity, e^* is the complex conjugate of the eigenvector, and \mathbf{r}^0 is the equilibrium position. α , b , and l represent the Cartesian direction, the atom index in a primitive cell, and the primitive cell index. We then use Eq. (5) to fit Eq. (3) to extract the anharmonic frequency ω^A and the linewidth Γ of the corresponding vibrational mode,

$$\Phi^F(\mathbf{k}, \omega)_s = \frac{c(\mathbf{k})_s}{[\omega - \omega^A(\mathbf{k})_s]^2 + [\frac{\Gamma(\mathbf{k})_s}{2}]^2}, \quad (5)$$

where c is a fitting parameter.

E. Interpolation for the frequency-dependent linewidth

The large computational cost required to obtain the linewidths required for WTE using the NMD method limits our ability to study large-size models with tens of thousands of atoms. To circumvent this limitation, we first employed the NMD method using a model containing 5832 atoms to extract the modal linewidths. Then, the following equations are used to obtain the frequency-dependent linewidth $\Gamma(\omega)$ [21,33,50]:

$$\Gamma(\omega) = \frac{1}{\sqrt{\frac{1}{\Gamma_1(\omega)^2} + \frac{1}{\Gamma_2(\omega)^2}}}, \quad (6)$$

where $\Gamma_1(\omega)$ and $\Gamma_2(\omega)$ are

$$\Gamma_1(\omega) = \frac{\sum_{\mathbf{k},s} \frac{1}{\sqrt{2\pi}\sigma^2} \exp\left[-\frac{[\omega(\mathbf{k})_s - \omega]^2}{2\sigma^2}\right]}{\sum_{\mathbf{k},s} \frac{1}{\Gamma(\mathbf{k})_s} \frac{1}{\sqrt{2\pi}\sigma^2} \exp\left[-\frac{[\omega(\mathbf{k})_s - \omega]^2}{2\sigma^2}\right]}, \quad (7)$$

$$\Gamma_2(\omega) = c_1 \omega^2 + c_2 \omega^4. \quad (8)$$

Specifically, we applied a Gaussian filter [Eq. (7)] on modal linewidths extracted using the NMD method to obtain a frequency-dependent relationship [$\Gamma_1(\omega)$]. Because of the limited sampling points in the low-frequency region, it is a common practice to employ $\Gamma_2(\omega)$ to correct the linewidths of low-frequency modes [21,33,50,51]. The parameters c_1 and c_2 are determined from the data points with frequencies lower than 8 rad ps⁻¹ using a least-square fitting. A larger frequency cutoff at 10 rad ps⁻¹ gave negligible differences in the results. The parameter c_2 is set to 0 to study the relation $\Gamma_2(\omega) = c\omega^2$. See Supplemental Material [52] (including Refs. [53–55]) Note A for more discussions about the accuracy of the relations $\Gamma_2(\omega) = c_1 \omega^2 + c_2 \omega^4$ and $\Gamma_2(\omega) = c\omega^2$.

III. RESULTS AND DISCUSSION

A. \mathbf{k} -mesh versus Gamma-point approaches in the WTE

Prior results [33] on the thermal conductivity of a-SiO₂ suggested that the WTE with a finite \mathbf{k} -mesh using finite-size models is accurate for temperatures larger than a lower bound (around 100 K), and that a regularization protocol is required to correctly evaluate the thermal conductivity below this temperature. However, a subsequent study [21] argued qualitatively that the \mathbf{k} -mesh approach might introduce artificially long-lived modes with low frequency, leading to a spurious increase in thermal conductivity. We investigated the above question with the a-Si system by comparing the WTE calcu-

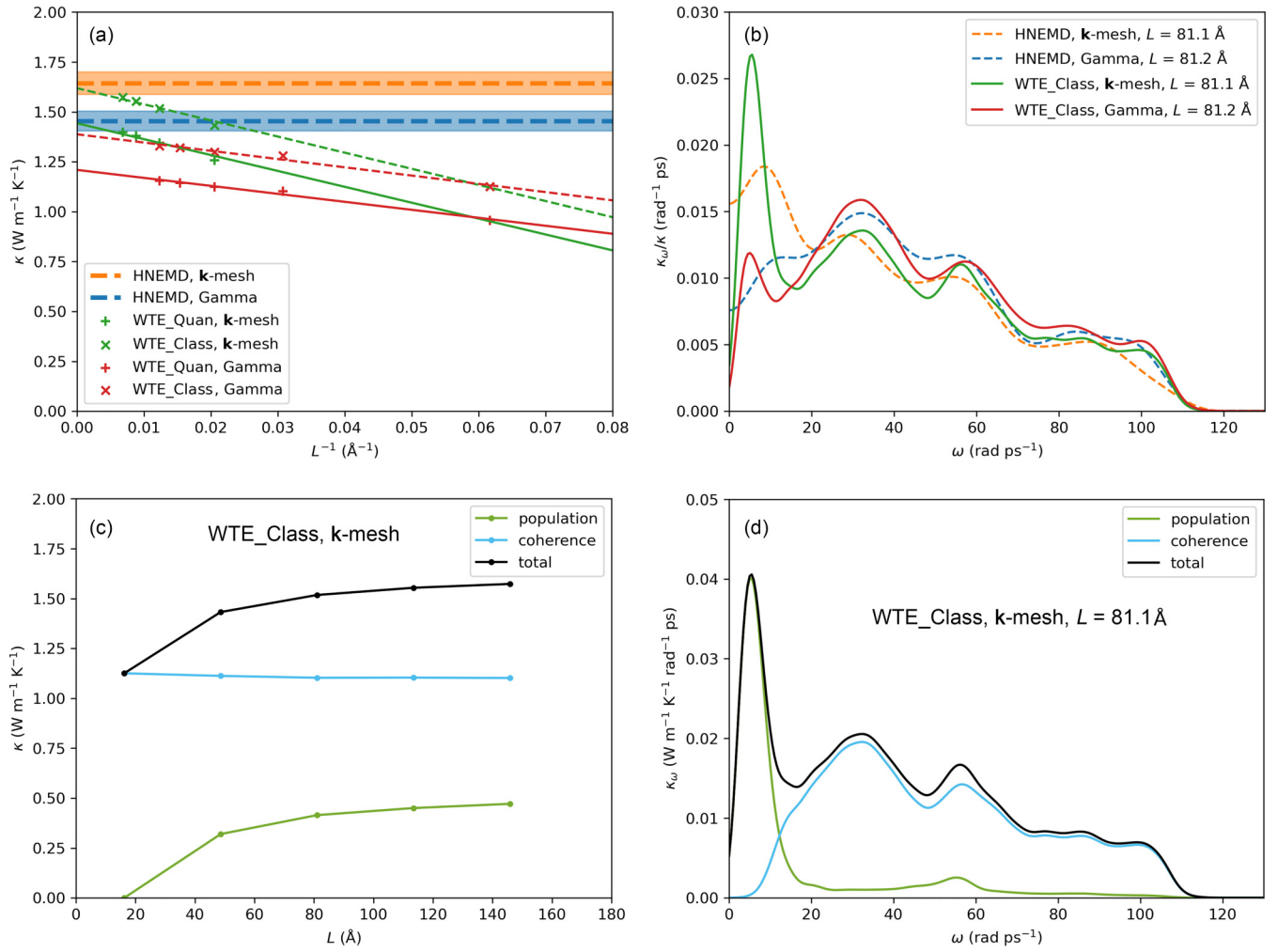


FIG. 1. Thermal conductivity of a-Si at 300 K using the k -mesh and Gamma-point approaches. (a) The comparison between the size-converged HNEMD results and WTE results at different sizes. The shaded area of HNEMD results indicates the uncertainty calculated from three independent simulations. Both quantum statistics and classical statistics are employed in WTE calculations. The solid lines and dashed lines are linear extrapolations from the data points in the WTE calculations to obtain the size-independent thermal conductivity. (b) Normalized spectral thermal conductivity of the HNEMD and classical WTE calculations at their corresponding sizes. (c) The size effects of the population- and coherence-channel thermal conductivity of the classical WTE calculations using the k -mesh approach. (d) The spectral decomposition of the WTE classical thermal conductivity obtained from the k -mesh approach for the 81.1 Å model with 27 000 atoms into the population and coherence channels.

lations with those from HNEMD simulations at 300 K. This comparison is appropriate as both results explicitly include anharmonicity and the WTE calculation can be performed using classical statistics to be consistent with the MD simulations. As the WTE requires modal linewidths and amorphous systems have no symmetry, performing anharmonic lattice dynamics to get the linewidths can be computationally prohibitive for models exceeding 10 000 atoms. To circumvent this limitation, we combined the MD-based NMD method [47–49] with an interpolation method [21,33,50] to extract the required modal linewidths (see Methods and Supplemental Material Note A [52]).

Figure S1 [52] contains the radial distribution function and DOS calculated using our models, which agree with previous simulation studies [8,13]. The calculated DOS, however, deviates from experiments, as also seen in earlier simulations [42,56]. This deviation is expected as most potentials

can only approximate the behavior of real-world materials. It is also well known that there is a large range of measured thermal conductivities for a-Si based on different film thickness and sample quality, so comparison with experiment would be difficult [57]. Thus, we only benchmarked results from the HNEMD with the WTE to ensure an equitable comparison, as both calculations are based on the same SW potential. From Fig. 1(a), a 300-K size-converged HNEMD thermal conductivity of 1.45 ± 0.01 W m⁻¹ K⁻¹ is obtained using the Gamma-point approach (i.e., supercells are obtained using the melt-quench technique). This result agrees with a prior nonequilibrium molecular dynamics result [58]. See Supplemental Material Note B [52] for discussion of the size-dependent HNEMD thermal conductivity and the comparison with results obtained using the EMD Green-Kubo approach.

We draw two significant conclusions from Fig. 1(a), where the WTE-calculated thermal conductivities are plotted versus

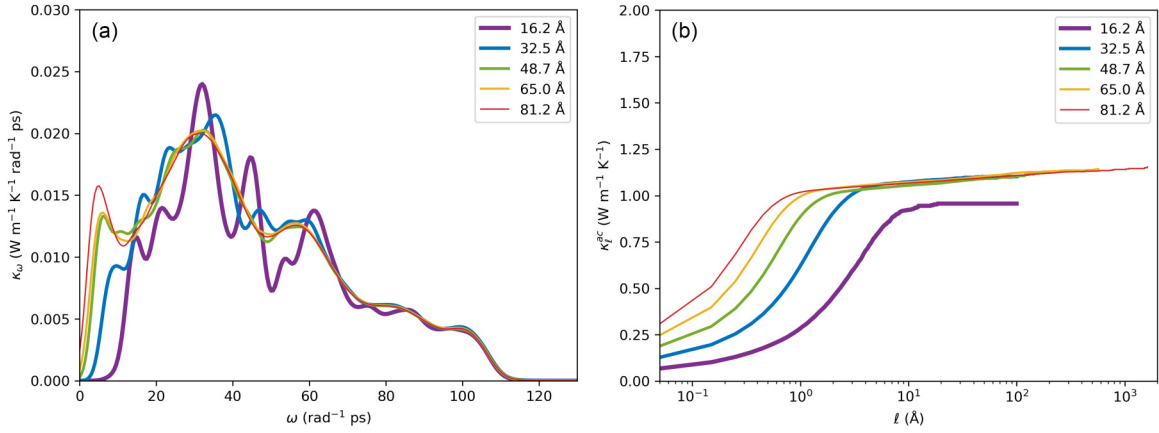


FIG. 2. The size dependence of (a) the spectral thermal conductivity and (b) the two-mode mean free path–dependent accumulative thermal conductivity at 300 K under quantum statistics.

the inverse of the simulation box length. First, when extrapolated to infinite size, the classical WTE thermal conductivities based on the \mathbf{k} -mesh and Gamma-point approaches agree well with the corresponding size-converged HNEMD results. This result is further discussed below. Second, the thermal conductivity results from the \mathbf{k} -mesh approach are higher than the Gamma-point approach in both the HNEMD and the WTE (classical and quantum) calculations. Comparing the normalized thermal conductivity spectra for the HNEMD and classical WTE approaches in Fig. 1(b) reveals that the discrepancy primarily stems from low-frequency vibrational modes that have higher contributions in the \mathbf{k} -mesh approach. For more insight, we decomposed the classical WTE \mathbf{k} -mesh thermal conductivity into its population channel and coherence channel in Figs. 1(c) and 1(d). These plots indicate that the increase in the thermal conductivity of the bigger supercells comes from the population channel [Fig. 1(c)], which displays a prominent spectral thermal conductivity peak at low frequencies [Fig. 1(d)]. A similar peak is also observed in the results for a larger a-Si model with 5832 atoms (Fig. S2 [52]), indicating that size effects are not impacting our conclusion. As a reminder, the population channel is contributed by vibrational modes at \mathbf{k} points other than the Gamma point, because Gamma-point modes of the primitive cell have zero modal group velocity due to symmetry constraints. The above observations imply that a considerable fraction of the thermal conductivity from low-frequency modes (up to $\sim 96\%$ for $\omega < 10 \text{ rad ps}^{-1}$) in the supercell models originates from the population channel, which is contributed by fictitious vibrational modes with wavelengths longer than the size of our simulated amorphous structures. These vibrational modes are induced by the imposed translational symmetry, raising concerns about the correctness of the \mathbf{k} -mesh approach. Hence, for the rest of this paper, we will only present the WTE results obtained from the Gamma-point approach.

B. Two-mode terms from WTE for describing thermal transport in amorphous silicon

Our classical WTE thermal conductivity values, when linearly extrapolated to infinite size in Fig. 1(a), agree well with the HNEMD results for both the \mathbf{k} -mesh and the Gamma-point approaches. However, a nonlinear extrapolation method

has been previously employed for a-Si [21]. This difference suggests that an investigation using a mode-level analysis is required, which can additionally clarify the mode-level carrier physics that are important for manipulating and engineering the thermal transport in amorphous materials. To investigate the underlying mode-level physics, we utilize the two-mode terms in the WTE. Inspired by an earlier work [29], we start by rewriting Eq. (1) into

$$\kappa = \sum_{\mathbf{k}} \sum_{s,s'} \kappa(\mathbf{k})_{s,s'} = \frac{1}{3V} \sum_{\mathbf{k}} \sum_{s,s'} C(\mathbf{k})_{s,s'} \|\mathbf{v}(\mathbf{k})_{s,s'}\|^2 \tau(\mathbf{k})_{s,s'}, \quad (9)$$

where the two-mode heat capacity and the two-mode lifetime are defined as $C(\mathbf{k})_{s,s'} = \frac{\omega(\mathbf{k})_s + \omega(\mathbf{k})_{s'}}{4} \left[\frac{C(\mathbf{k})_s}{\omega(\mathbf{k})_s} + \frac{C(\mathbf{k})_{s'}}{\omega(\mathbf{k})_{s'}} \right]$ and $\tau(\mathbf{k})_{s,s'} = \frac{(\Gamma(\mathbf{k})_s + \Gamma(\mathbf{k})_{s'})/2}{(\omega(\mathbf{k})_s - \omega(\mathbf{k})_{s'})^2 + (\Gamma(\mathbf{k})_s + \Gamma(\mathbf{k})_{s'})^2/4}$. The two-mode mean free path is accordingly defined as $\ell(\mathbf{k})_{s,s'} = \|\mathbf{v}(\mathbf{k})_{s,s'}\| \tau(\mathbf{k})_{s,s'}$. The spectral thermal conductivity and the two-mode mean free path–dependent accumulative thermal conductivity at 300 K under quantum statistics plotted in Fig. 2 reveal that thermal conductivity increases with increasing size due to the presence of more low-frequency modes with longer two-mode mean free paths. Based on this observation, we would expect the modal properties to also converge when properly extrapolated to infinite size. To validate this hypothesis, we convert Eq. (9) to a frequency-dependent form for easier extrapolation of the transport properties of the lower frequency modes that are unavailable due to our model size:

$$\begin{aligned} \kappa &= \int_0^{\omega_{\max}} \int_0^{\omega_{\max}} \kappa_{\omega,\omega'} d\omega d\omega' \\ &= \frac{1}{3V} \int_0^{\omega_{\max}} \int_0^{\omega_{\max}} N_{\omega,\omega'} C_{\omega,\omega'} \|\mathbf{v}_{\omega,\omega'}\|^2 \tau_{\omega,\omega'} d\omega d\omega', \quad (10) \end{aligned}$$

where the frequency-dependent two-mode DOS $N_{\omega,\omega'} = \sum_{s,s'} \tilde{\delta}(\omega_s - \omega, \omega_{s'} - \omega')$. $\tilde{\delta}(\omega_s - \omega, \omega_{s'} - \omega')$ is a rectangular approximation to a two-dimensional δ function centered at discrete frequencies (ω, ω') with a width equal to 1 rad ps^{-1} . The frequency-dependent two-mode group velocity is defined as $\|\mathbf{v}_{\omega,\omega'}\| = \sum_{s,s'} \|\mathbf{v}_{s,s'}\| \tilde{\delta}(\omega_s - \omega, \omega_{s'} - \omega') / N_{\omega,\omega'}$, while $C_{\omega,\omega'}$ and $\tau_{\omega,\omega'}$ are the frequency-dependent two-mode heat capacity and lifetime, with similar definitions as $\|\mathbf{v}_{\omega,\omega'}\|$.

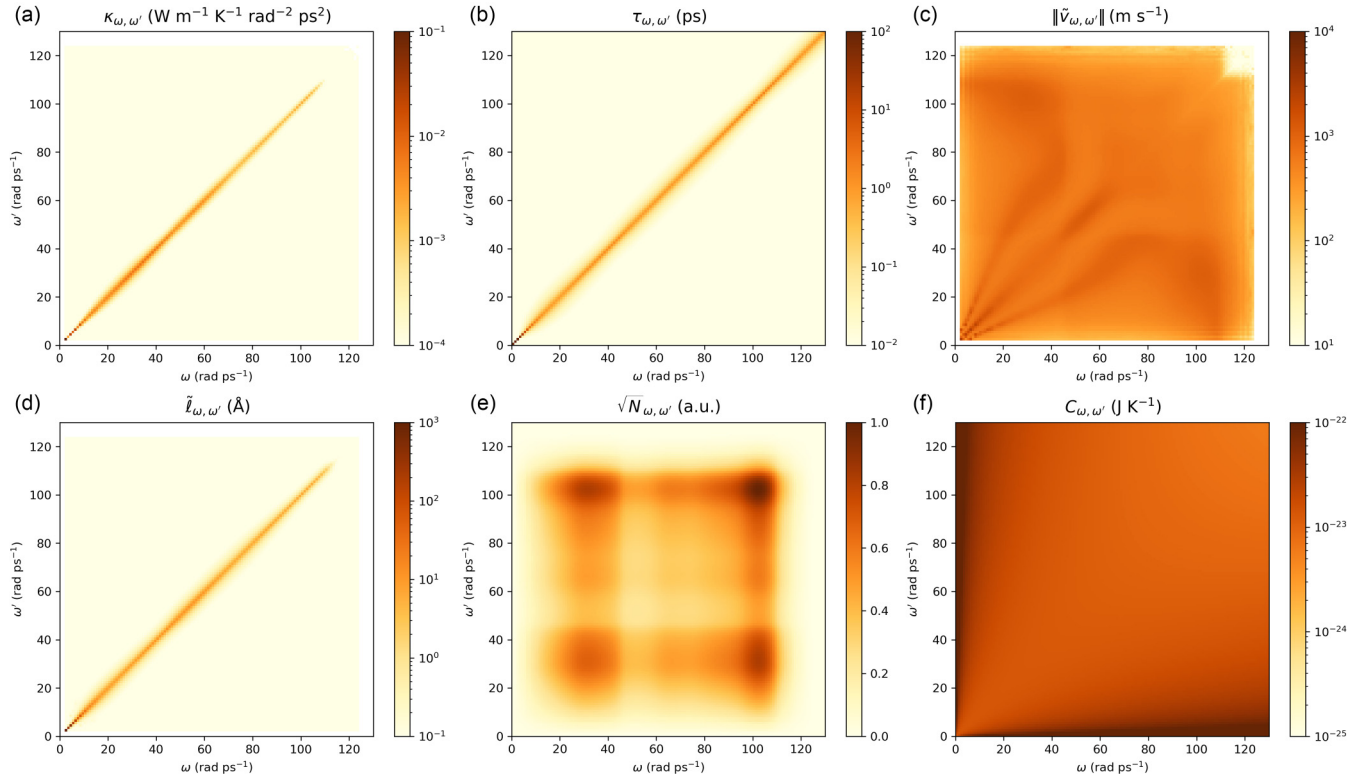


FIG. 3. Frequency-dependent two-mode properties of a-Si at 300 K. (a)–(f) The frequency-dependent two-mode thermal conductivity, lifetime, size-invariant group velocity, size-invariant mean free path, square root of DOS, and heat capacity at 300 K under quantum statistics.

It is notable that the $\|\mathbf{v}_{\omega,\omega'}\|$ terms are dependent on V , creating an inconsistency for thermal conductivity predictions when models with different sizes are used (see Supplemental Material Note C [52]). Therefore, we define a size-invariant frequency-dependent two-mode group velocity as $\tilde{\mathbf{v}}_{\omega,\omega'} = \mathbf{v}_{\omega,\omega'} N_{\omega,\omega'}^{1/4}$ (see Supplemental Material Note C [52]). Equation (10) can then be recast into

$$\kappa = \frac{1}{3V} \int_0^{\omega_{\max}} \int_0^{\omega_{\max}} \sqrt{N_{\omega,\omega'}} C_{\omega,\omega'} \|\tilde{\mathbf{v}}_{\omega,\omega'}\|^2 \tau_{\omega,\omega'} d\omega d\omega'. \quad (11)$$

Accordingly, the size-invariant frequency-dependent two-mode mean free path is given as $\tilde{\ell}_{\omega,\omega'} = \|\tilde{\mathbf{v}}_{\omega,\omega'}\| \tau_{\omega,\omega'}$. Using the above frequency-dependent two-mode terms and the Gamma-point approach, the frequency-dependent two-mode properties of a-Si at the temperature of 300 K under quantum statistics are illustrated in Fig. 3. The nonzero thermal conductivity contribution of the two-mode terms in Fig. 3(a) closely mirrors their lifetime in Fig. 3(b). This similarity arises as the two-mode lifetimes depend on the linewidth overlap of the two coupling vibrational modes. Thus, two-mode terms with significantly different frequencies will have a negligible two-mode lifetime.

As the lowest nonzero frequency in our largest model is 2.68 rad ps^{-1} , the properties of lower frequency vibrational modes are extrapolated to obtain a more accurate thermal conductivity prediction (see Supplemental Material Note D [52] for details of the extrapolation procedure). Including contributions from the extrapolated modes, the κ calculated using Eq. (11) under classical statistics is $1.40 \text{ W m}^{-1} \text{ K}^{-1}$.

This value agrees well with the $1.39 \text{ W m}^{-1} \text{ K}^{-1}$ from linear extrapolation of κ to infinite size [i.e., red crosses in Fig. 1(a)] and the HNEMD value of $1.45 \text{ W m}^{-1} \text{ K}^{-1}$ [i.e., blue line in Fig. 1(a)]. The κ under quantum statistics is $1.25 \text{ W m}^{-1} \text{ K}^{-1}$ versus $1.21 \text{ W m}^{-1} \text{ K}^{-1}$ [linear extrapolation of κ to infinite size, indicated by the red plus signs in Fig. 1(a)]. The close agreement between these results supports the credibility of our method using the two-mode terms, ensuring a consistent calculation approach under one framework with no need to invoke the concept of propagons and Eq. (2) to calculate thermal conductivity.

C. Connections between the two-mode terms and propagons, diffusons, and locons

Propagons are commonly used to recover the contributions from the low-frequency vibrational modes that are inaccessible due to the limited size of amorphous models [8,9,21]. By comparing Eq. (11) with the κ_P in Eq. (2), we identified that the contribution from propagons is only similar to that from the two-mode terms along the diagonal. In addition, the former adopts a constant sound speed when calculating the thermal conductivity. This assumption, however, does not always hold true, particularly when anharmonicity is large [28,30] and/or when a large crossover frequency is used to distinguish propagons from diffusons. The two-mode terms in the low-frequency range can have a size-invariant group velocity exceeding 1000 m s^{-1} and a lifetime longer than 100 ps, resulting in two-mode mean free paths up to 1000 Å [Figs. 3(b)–3(d)]. These features underscore their “propagating” characteristics. In addition, the two-mode terms in the

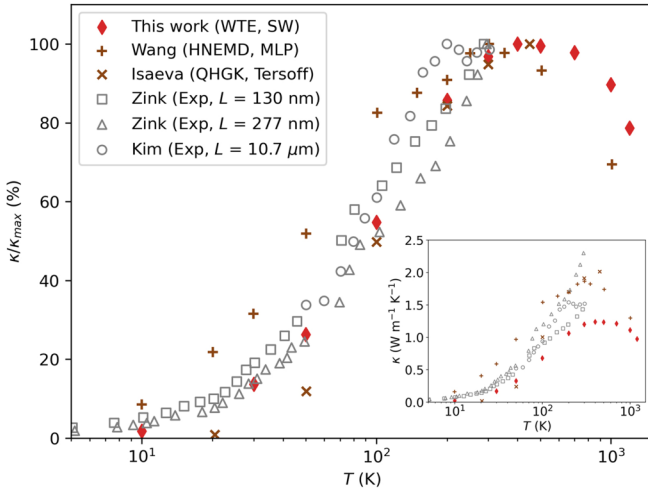


FIG. 4. Temperature-dependent thermal conductivity of a-Si. The thermal conductivity values in each study are normalized to their highest value (κ_{\max}) across the temperature range, with absolute values shown in the inset. Our Gamma-point WTE results, the HNEMD results of Wang *et al.*, and Isaeva’s QHKG results are based on the SW potential, a machine learning potential (MLP) [62], and the Tersoff potential [29], respectively. The WTE and QHKG results use quantum statistics, while the HNEMD results are quantum corrected. Experiments are taken from Refs. [60,61] with the sample thicknesses provided in the legend.

high-frequency range exhibit an approximately zero group velocity [Fig. 3(c)], accordingly negligible mean free path [Fig. 3(d)], and thermal conductivity [Fig. 3(a)], suggest-

ing they are “Anderson localized” [33,59]. The two-mode terms between the above frequency ranges can be treated as “diffusive” in nature. Thus, the spectrum of two-mode terms has characteristics that resemble those of the three heat carriers typically used to describe amorphous materials. We emphasize that we are not attempting to classify the different two-mode terms into these three heat carriers. Rather, we seek to demonstrate that the WTE theory naturally encompasses contributions from all vibrational modes, and the total thermal conductivity can be obtained without classifying them into propagons, diffusons, and locons.

D. Two-mode terms elucidate physics behind the anomalous high-temperature thermal conductivity trend in some amorphous materials

We now explore how increased anharmonicity in amorphous materials is captured in the two-mode properties in the WTE. In Fig. 4, the temperature dependence of the thermal conductivity of a-Si is plotted for our quantum Gamma-point WTE calculations, using models with 5832 atoms and incorporating extrapolated low-frequency contributions. In the main part of the plot, thermal conductivity is normalized by the maximum value calculated or measured, while the inset contains the actual values. Previous experiments [60,61] and calculations performed using other potentials and approaches [29,62] generally agree well with our normalized trend. Any discrepancies are probably due to the different potentials and computational structures used [57]. An intriguing observation from Fig. 4 is the anomalous thermal conductivity peak at around 400 K. A similar high-temperature peak was reported

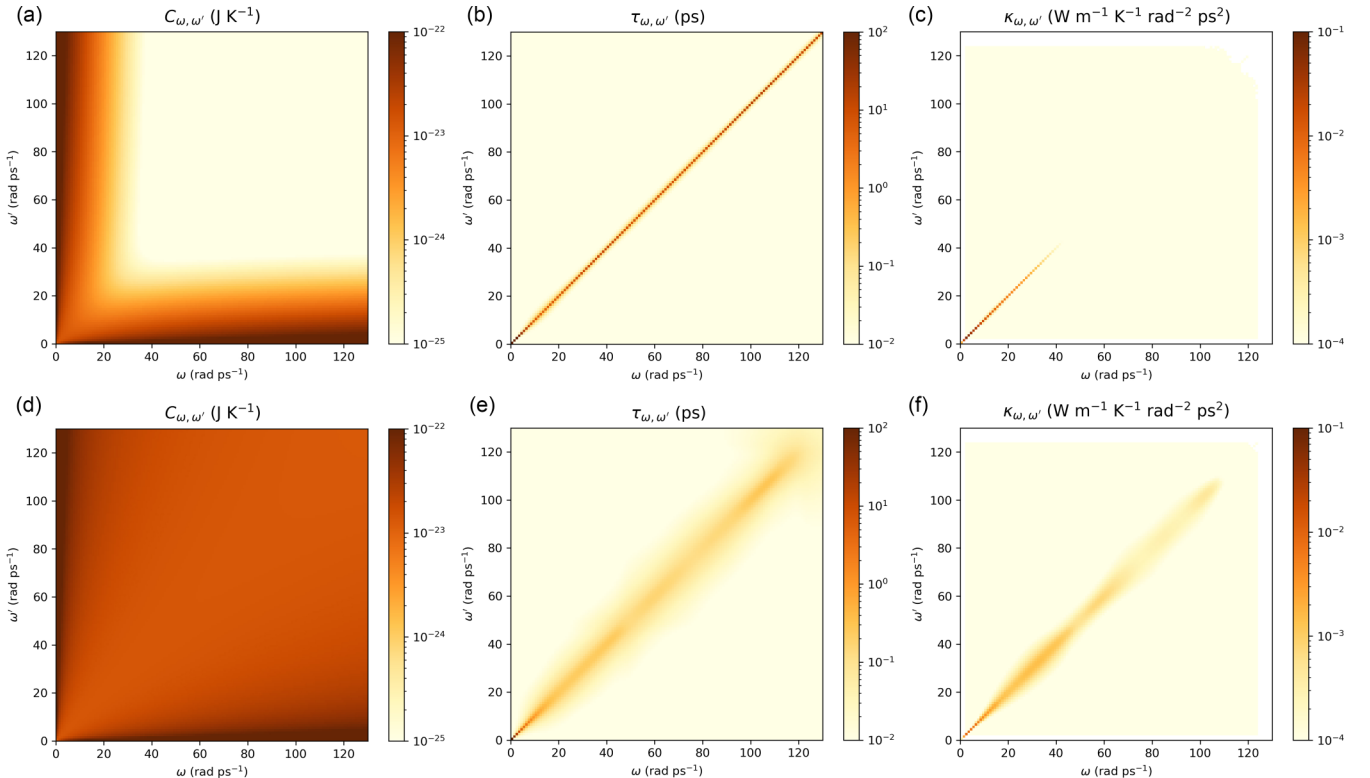


FIG. 5. Frequency-dependent two-mode $C_{\omega,\omega'}$, $\tau_{\omega,\omega'}$, and $\kappa_{\omega,\omega'}$ for a-Si at temperatures of (a)–(c) 30 K and (d)–(f) 1000 K. These variables have the same meaning as those in Figs. 3(f), 3(b), and 3(a), respectively.

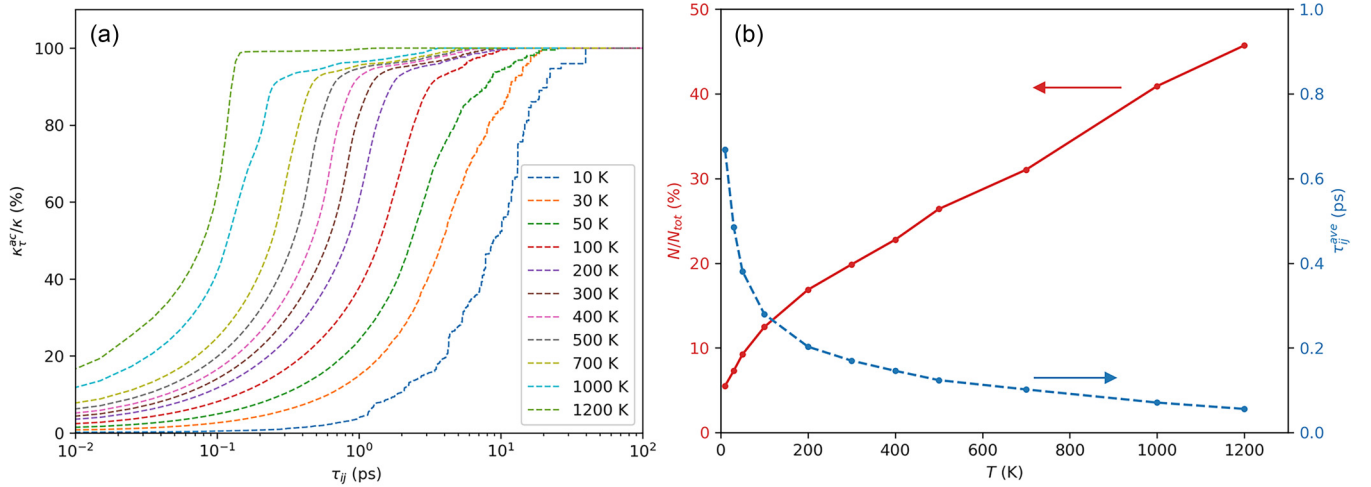


FIG. 6. The temperature dependence of (a) two-mode lifetime-dependent accumulative thermal conductivity ($\kappa_{\tau}^{\text{ac}}$) normalized by its maximum κ and (b) the percentage of contributing two-mode elements and the average two-mode lifetime of these contributing elements. The red solid line in (b) (left axis) illustrates changes in the percentage of contributing two-mode elements over the total number of two-mode elements (N/N_{tot}) at different temperatures. The blue dashed line (right axis) represents changes in the average two-mode lifetime τ_{ij}^{ave} of the contributing elements across temperatures.

in recent theoretical studies for a-Si and amorphous HfO_2 (a-HfO₂) [62,63], which challenges the conventional notion that the thermal conductivity for amorphous materials increases with increasing temperature [5–7]. Such a peak, however, has not been observed in a-SiO₂ [33,64]. The origin of the peak can be explained using the two-mode terms in the WTE.

Figure 5 illustrates the two-mode properties of a-Si at temperatures of 30 and 1000 K. Given that our linewidths are from the classical NMD method, they may deviate from the quantum case at low temperatures. However, such deviations become mostly immaterial when using the quantum heat capacity [Fig. 5(a)] for calculating the two-mode thermal conductivity [Fig. 5(c)] [62]. As there are small differences between the two-mode lifetimes at 300 K in Fig. 3(b) and at 30 K in Fig. 5(b), the thermal conductivity of a-Si at 30 K is dictated primarily by its smaller heat capacity [comparing Figs. 3(f) and 5(a)] and not the linewidths. At 1000 K, however, most of the two-mode elements are activated as seen from the heat capacity plot in Fig. 5(d). In addition, as expected, a higher number of two-mode elements at the elevated temperature display a nonzero lifetime in Fig. 5(e). This increase comes from the stronger anharmonicity, which broadens the linewidths, allowing more vibrational modes with larger dissimilar frequencies to couple. When comparing the two-mode lifetimes at 300 K in Fig. 3(b) and 1000 K in Fig. 5(e), however, the color for two-mode elements active at 300 K becomes less intense at 1000 K, indicating a decrease in the lifetime. This drop in the two-mode lifetime with increasing temperatures can be clearly seen in the normalized accumulated thermal conductivity curves plotted in Fig. 6(a). Two-mode elements with a shorter lifetime dominate the thermal transport at higher temperatures.

In Fig. 6(b), we compare the percentage of the contributing two-mode elements and the average lifetime of the contributing two-mode elements across temperatures to identify

two competing trends. A contributing two-mode element is defined here using the criterion $\tau_{ij} > 0.01$ ps. Two-mode elements that satisfy this criterion contribute more than 90% to the total thermal conductivity from 10 to 1000 K and around 88% at 1200 K. These results are not affected if a smaller criterion for τ_{ij} is adopted at 1200 K to ensure a 90% contribution. Although the number of contributing two-mode elements increases with increasing temperatures, the average two-mode lifetime of these contributing two-mode elements decreases. The latter effect dominates in a-Si to decrease its high-temperature thermal conductivity. We postulate that the decrease in the two-mode lifetimes is also responsible for the trend in a-HfO₂ at higher temperatures [63]. In contrast, these two competing trends possibly balance out in a-SiO₂, leaving its total thermal conductivity unchanged [33,64].

IV. CONCLUSION

In summary, we explored issues surrounding thermal transport in amorphous materials using theoretical calculations on a-Si. We first showed that the \mathbf{k} -mesh approach introduces fictitious translational symmetry leading to an overprediction of thermal conductivity. We proceed to use the two-mode terms in the WTE theory to derive a frequency-dependent formula tailored for amorphous materials, which effectively captures thermal conductivity contributions from low-frequency vibrational modes that exceed the limitations of the model size. In addition, we argue that classifying the modes as propagons, diffusons, and locons is not necessary, as their characteristics are naturally captured through the two-mode properties in WTE. We also identified the mechanisms behind the anomalous high-temperature thermal conductivity decrease in amorphous materials. Our study provides insights for identifying new thermal transport physics and developing new methodologies to manipulate thermal transport in amorphous materials.

ACKNOWLEDGMENTS

This paper is based upon work supported by the National Natural Science Foundation of China (Grant No. 52350610259), a SUTD-ZJU IDEA Visiting Professor grant [Grant No. SUTD-ZJU (VP) 202001], Zhejiang University Global Partnership Fund, and the Zhejiang-Saudi Energy Materials International Collaboration Laboratory. X.Z. acknowledges support from the National Natural Science Foundation of China (Grant No. 12005019).

J.Y. and W.L.O. originated the research. J.Y. performed all the calculations. J.Y. and W.L.O. analyzed the results and

wrote the manuscript. All authors studied, commented, and edited the manuscript.

The authors declare that they have no known competing financial interests.

DATA AVAILABILITY

Further data that support the plots within this paper as well as other findings of this study are available from the corresponding author upon reasonable request. Source data are provided with this paper. Codes for reproducing the calculation results are available from the corresponding author upon reasonable request.

-
- [1] D. Geng, K. Wang, L. Li, K. Myny, A. Nathan, J. Jang, Y. Kuo, and M. Liu, Thin-film transistors for large-area electronics, *Nat. Electron.* **6**, 963 (2023).
 - [2] W. Liu *et al.*, Light-induced activation of boron doping in hydrogenated amorphous silicon for over 25% efficiency silicon solar cells, *Nat. Energy* **7**, 427 (2022).
 - [3] W. Zhou, Y. Cheng, K. Chen, G. Xie, T. Wang, and G. Zhang, Thermal conductivity of amorphous materials, *Adv. Funct. Mater.* **30**, 1903829 (2020).
 - [4] P.-H. Huang *et al.*, Three-dimensional printing of silica glass with sub-micrometer resolution, *Nat. Commun.* **14**, 3305 (2023).
 - [5] P. B. Allen and J. L. Feldman, Thermal conductivity of glasses: Theory and application to amorphous Si, *Phys. Rev. Lett.* **62**, 645 (1989).
 - [6] P. B. Allen and J. L. Feldman, Thermal conductivity of disordered harmonic solids, *Phys. Rev. B* **48**, 12581 (1993).
 - [7] J. L. Feldman, M. D. Kluge, P. B. Allen, and F. Wooten, Thermal conductivity and localization in glasses: Numerical study of a model of amorphous silicon, *Phys. Rev. B* **48**, 12589 (1993).
 - [8] P. B. Allen, J. L. Feldman, J. Fabian, and F. Wooten, Diffusons, locons and propagons: Character of atomic vibrations in amorphous Si, *Philos. Mag. B* **79**, 1715 (1999).
 - [9] J. L. Feldman, P. B. Allen, and S. R. Bickham, Numerical study of low-frequency vibrations in amorphous silicon, *Phys. Rev. B* **59**, 3551 (1999).
 - [10] J. L. Feldman, Calculations of the generalized dynamic structure factor for amorphous silicon, *J. Non-Cryst. Solids* **307**, 128 (2002).
 - [11] S. Shenogin, A. Bodapati, P. Keblinski, and A. J. H. McGaughey, Predicting the thermal conductivity of inorganic and polymeric glasses: The role of anharmonicity, *J. Appl. Phys.* **105**, 034906 (2009).
 - [12] Y. He, D. Donadio, and G. Galli, Heat transport in amorphous silicon: Interplay between morphology and disorder, *Appl. Phys. Lett.* **98**, 144101 (2011).
 - [13] J. M. Larkin and A. J. H. McGaughey, Thermal conductivity accumulation in amorphous silica and amorphous silicon, *Phys. Rev. B* **89**, 144303 (2014).
 - [14] L. Yang, N. Yang, and B. Li, Extreme low thermal conductivity in nanoscale 3D Si phononic crystal with spherical pores, *Nano Lett.* **14**, 1734 (2014).
 - [15] W. Lv and A. Henry, Direct calculation of modal contributions to thermal conductivity via Green-Kubo modal analysis, *New J. Phys.* **18**, 013028 (2016).
 - [16] H. R. Seyf and A. Henry, A method for distinguishing between propagons, diffusions, and locons, *J. Appl. Phys.* **120**, 025101 (2016).
 - [17] J. Moon, B. Latour, and A. J. Minnich, Propagating elastic vibrations dominate thermal conduction in amorphous silicon, *Phys. Rev. B* **97**, 024201 (2018).
 - [18] H. R. Seyf, W. Lv, A. Rohskopf, and A. Henry, The importance of phonons with negative phase quotient in disordered solids, *Sci. Rep.* **8**, 2627 (2018).
 - [19] F. DeAngelis, M. G. Muraleedharan, J. Moon, H. R. Seyf, A. J. Minnich, A. J. H. McGaughey, and A. Henry, Thermal transport in disordered materials, *Nanoscale Microscale Thermophys. Eng.* **23**, 81 (2019).
 - [20] J. Moon, Examining normal modes as fundamental heat carriers in amorphous solids: The case of amorphous silicon, *J. Appl. Phys.* **130**, 055101 (2021).
 - [21] A. Fiorentino, P. Pegolo, and S. Baroni, Hydrodynamic finite-size scaling of the thermal conductivity in glasses, *npj Comput. Mater.* **9**, 157 (2023).
 - [22] Y. Liao and J. Shiomi, Akhiezer mechanism dominates relaxation of propagons in amorphous material at room temperature, *J. Appl. Phys.* **130**, 035101 (2021).
 - [23] W. Lv and A. Henry, Non-negligible contributions to thermal conductivity from localized modes in amorphous silicon dioxide, *Sci. Rep.* **6**, 35720 (2016).
 - [24] P. Norouzzadeh, C. W. Myles, and D. Vashae, Phonon dynamics in type-VIII silicon clathrates: Beyond the rattler concept, *Phys. Rev. B* **95**, 195206 (2017).
 - [25] B. Li, F. DeAngelis, G. Chen, and A. Henry, The importance of localized modes spectral contribution to thermal conductivity in amorphous polymers, *Commun. Phys.* **5**, 323 (2022).
 - [26] Z. Cai, S. Lin, and C. Zhao, Anomalous diffuson and locon-dominated Wigner multi-channel thermal transport in disordered and shear-aligned polymers, *Macromolecules* **57**, 6209 (2024).
 - [27] R. J. Hardy, Energy-flux operator for a lattice, *Phys. Rev.* **132**, 168 (1963).
 - [28] M. Simoncelli, N. Marzari, and F. Mauri, Unified theory of thermal transport in crystals and glasses, *Nat. Phys.* **15**, 809 (2019).
 - [29] L. Isaeva, G. Barbalinardo, D. Donadio, and S. Baroni, Modeling heat transport in crystals and glasses from a unified lattice-dynamical approach, *Nat. Commun.* **10**, 3853 (2019).
 - [30] M. Simoncelli, N. Marzari, and F. Mauri, Wigner formulation of thermal transport in solids, *Phys. Rev. X* **12**, 041011 (2022).

- [31] A. Pazhedath, L. Bastonero, N. Marzari, and M. Simoncelli, First-principles characterization of thermal conductivity in LaPO_4 -based alloys, *Phys. Rev. Appl.* **22**, 024064 (2024).
- [32] A. F. Harper, K. Iwanowski, W. C. Witt, M. C. Payne, and M. Simoncelli, Vibrational and thermal properties of amorphous alumina from first principles, *Phys. Rev. Mater.* **8**, 043601 (2024).
- [33] M. Simoncelli, F. Mauri, and N. Marzari, Thermal conductivity of glasses: First-principles theory and applications, *npj Comput. Mater.* **9**, 106 (2023).
- [34] L. Yang and B.-Y. Cao, Significant anharmonicity of thermal transport in amorphous silica at high temperature, *Phys. Status Solidi RRL* **16**, 2200217 (2022).
- [35] A. Fiorentino, E. Drigo, S. Baroni, and P. Pegolo, Unearthing the foundational role of anharmonicity in heat transport in glasses, *Phys. Rev. B* **109**, 224202 (2024).
- [36] F. H. Stillinger and T. A. Weber, Computer simulation of local order in condensed phases of silicon, *Phys. Rev. B* **31**, 5262 (1985).
- [37] G. Caldarelli, M. Simoncelli, N. Marzari, F. Mauri, and L. Benfatto, Many-body Green's function approach to lattice thermal transport, *Phys. Rev. B* **106**, 024312 (2022).
- [38] A. Fiorentino and S. Baroni, From Green-Kubo to the full Boltzmann kinetic approach to heat transport in crystals and glasses, *Phys. Rev. B* **107**, 054311 (2023).
- [39] X. Li, S. Thébaud, and L. Lindsay, Primitive to conventional geometry projection for efficient phonon transport calculations, *npj Comput. Mater.* **9**, 193 (2023).
- [40] S. Plimpton, Fast parallel algorithms for short-range molecular dynamics, *J. Comput. Phys.* **117**, 1 (1995).
- [41] A. P. Thompson *et al.*, LAMMPS - a flexible simulation tool for particle-based materials modeling at the atomic, meso, and continuum scales, *Comput. Phys. Commun.* **271**, 108171 (2022).
- [42] K. Laaziri, S. Kycia, S. Roorda, M. Chicoine, J. L. Robertson, J. Wang, and S. C. Moss, High-energy x-ray diffraction study of pure amorphous silicon, *Phys. Rev. B* **60**, 13520 (1999).
- [43] Z. Fan, H. Dong, A. Harju, and T. Ala-Nissila, Homogeneous nonequilibrium molecular dynamics method for heat transport and spectral decomposition with many-body potentials, *Phys. Rev. B* **99**, 064308 (2019).
- [44] Z. Fan, W. Chen, V. Vierimaa, and A. Harju, Efficient molecular dynamics simulations with many-body potentials on graphics processing units, *Comput. Phys. Commun.* **218**, 10 (2017).
- [45] A. Togo, First-principles phonon calculations with Phonopy and Phono3py, *J. Phys. Soc. Jpn.* **92**, 012001 (2023).
- [46] A. Togo, L. Chaput, T. Tadano, and I. Tanaka, Implementation strategies in phonopy and phono3py, *J. Phys.: Condens. Matter* **35**, 353001 (2023).
- [47] J. A. Thomas, J. E. Turney, R. M. Iutzi, C. H. Amon, and A. J. H. McGaughey, Predicting phonon dispersion relations and lifetimes from the spectral energy density, *Phys. Rev. B* **81**, 081411(R) (2010).
- [48] J. M. Larkin, J. E. Turney, A. D. Massicotte, C. H. Amon, and A. J. H. McGaughey, Comparison and evaluation of spectral energy methods for predicting phonon properties, *J. Comput. Theor. Nanosci.* **11**, 249 (2014).
- [49] T. Feng, B. Qiu, and X. Ruan, Anharmonicity and necessity of phonon eigenvectors in the phonon normal mode analysis, *J. Appl. Phys.* **117**, 195102 (2015).
- [50] S. Thébaud, T. Berlijn, and L. Lindsay, Perturbation theory and thermal transport in mass-disordered alloys: Insights from Green's function methods, *Phys. Rev. B* **105**, 134202 (2022).
- [51] S. Kwon, J. Zheng, M. C. Wingert, S. Cui, and R. Chen, Unusually high and anisotropic thermal conductivity in amorphous silicon nanostructures, *ACS Nano* **11**, 2470 (2017).
- [52] See Supplemental Material at <http://link.aps.org/supplemental/10.1103/PhysRevB.111.094206> for radial distribution functions and density of states of different models; size effects on thermal conductivity calculations; details of the low-frequency linewidth extrapolation; comparison between size-dependent HNEMD and EMD thermal conductivity; size effects of the frequency-dependent two-mode group velocity; and details of the low-frequency two-mode properties extrapolation.
- [53] D. Surblys, H. Matsubara, G. Kikugawa, and T. Ohara, Application of atomic stress to compute heat flux via molecular dynamics for systems with many-body interactions, *Phys. Rev. E* **99**, 051301(R) (2019).
- [54] P. Boone, H. Babaei, and C. E. Wilmer, Heat flux for many-body interactions: Corrections to LAMMPS, *J. Chem. Theory Comput.* **15**, 5579 (2019).
- [55] Z. Fan, Luiz Felipe C. Pereira, H.-Q. Wang, J.-C. Zheng, D. Donadio, and A. Harju, Force and heat current formulas for many-body potentials in molecular dynamics simulations with applications to thermal conductivity calculations, *Phys. Rev. B* **92**, 094301 (2015).
- [56] W. A. Kamitakahara, C. M. Soukoulis, H. R. Shanks, U. Buchenau, and G. S. Grest, Vibrational spectrum of amorphous silicon: Experiment and computer simulation, *Phys. Rev. B* **36**, 6539 (1987).
- [57] J. L. Braun, C. H. Baker, A. Giri, M. Elahi, K. Artyushkova, T. E. Beechem, P. M. Norris, Z. C. Leseman, J. T. Gaskins, and P. E. Hopkins, Size effects on the thermal conductivity of amorphous silicon thin films, *Phys. Rev. B* **93**, 140201(R) (2016).
- [58] Y. Zhou and M. Hu, Quantitatively analyzing phonon spectral contribution of thermal conductivity based on nonequilibrium molecular dynamics simulations. II. From time Fourier transform, *Phys. Rev. B* **92**, 195205 (2015).
- [59] P. W. Anderson, Absence of diffusion in certain random lattices, *Phys. Rev.* **109**, 1492 (1958).
- [60] B. L. Zink, R. Pietri, and F. Hellman, Thermal conductivity and specific heat of thin-film amorphous silicon, *Phys. Rev. Lett.* **96**, 055902 (2006).
- [61] T. Kim, J. Moon, and A. J. Minnich, Origin of micrometer-scale propagation lengths of heat-carrying acoustic excitations in amorphous silicon, *Phys. Rev. Mater.* **5**, 065602 (2021).
- [62] Y. Wang, Z. Fan, P. Qian, M. A. Caro, and T. Ala-Nissila, Quantum-corrected thickness-dependent thermal conductivity in amorphous silicon predicted by machine learning molecular dynamics simulations, *Phys. Rev. B* **107**, 054303 (2023).
- [63] H. Zhang, X. Gu, Z. Fan, and H. Bao, Vibrational anharmonicity results in decreased thermal conductivity of amorphous HfO_2 at high temperature, *Phys. Rev. B* **108**, 045422 (2023).
- [64] X. Zhu and C. Shao, Effect of anharmonicity on the thermal conductivity of amorphous silica, *Phys. Rev. B* **106**, 014305 (2022).